AN IMPROVED PUSHBROOM SCANNER MODEL FOR PRECISE GEOREFERENCING OF ALOS PRISM IMAGERY

T. Weser*, F. Rottensteiner, J. Willneff, C. S. Fraser

Cooperative Research Centre for Spatial Information, Department of Geomatics, The University of Melbourne, VIC 3010, Australia - (tweser, franzr, c.fraser)@unimelb.edu.au, jwillneff@web.de

Commission I, WG I / 5

KEY WORDS: ALOS PRISM, pushbroom, high-resolution, satellite, orientation

ABSTRACT:

One of the instruments on board of the ALOS satellite, launched by the Japanese Aerospace Exploration Agency (JAXA) in 2006, is the Panchromatic Remote-sensing Instrument for Stereo Mapping (PRISM). PRISM has three cameras with different viewing directions (nadir, forward, backward), recording imagery with a ground resolution of 2.5 m. A main characteristic of raw ALOS PRISM imagery is that depending on the observation mode each scene is split into four or six separate strips, each related to an individual CCD chip. Basic imagery is delivered as one image data file per strip. We have developed a pushbroom sensor model that is capable of dealing with individual CCD chips sharing some orientation parameters and that can thus be applied to ALOS PRISM imagery. It has previously been shown that pixel-level results can be achieved for georeferencing of ALOS PRISM imagery using this sensor model and a moderate number of ground control points. However, the distribution of resulting residuals suggested that the parameters describing the relative alignment of the individual CCD chips provided by JAXA might not be perfect. Thus, the sensor model was expanded to be capable of self-calibration of these CCD alignment parameters. In this paper, the sensor model will be outlined and the new self-calibration technique described. The effectiveness of self-calibration will be assessed as well as the calibration process carried out by JAXA, in the latter case comparing a set of CCD alignment parameters calibrated in October 2006, and thus representing a very early stage of system calibration, to an updated parameter set obtained in July 2007. Three scenes (forward, backward, nadir) covering a test field in Melbourne (Australia), consisting of more then 100 points surveyed by kinematic GPS, were used for this assessment. Our results show that self-calibration changes the relative alignment of the CCD chips by up to two pixels. If the original calibration data are used, self-calibration can improve the accuracy of the results by 33% and from pixel-level to sub-pixel level. The updated calibration parameters provided by JAXA yield considerably better results than the original ones. In this case, self-calibration essentially helps to increase the height accuracy by about 20%.

1. INTRODUCTION

The Advanced Land Observing Satellite (ALOS) was launched by the Japanese Aerospace Exploration Agency (JAXA) in 2006. One of the instruments on board ALOS is the Panchromatic Remote-sensing Instrument for Stereo Mapping (PRISM). PRISM has three cameras with different viewing directions (nadir, forward, backward), recording 8 bit panchromatic imagery with a ground resolution of 2.5 m. Each camera consists of six or eight separate CCD chips. Depending on the observation mode, either four or six of these CCD chips are used to record a scene. Raw PRISM imagery (level 1B1 data) is thus delivered in the form of four or six image data files (one per CCD chip). These files also contain information about the satellite orbit and the camera viewing angles (JAXA, 2006). Interior orientation parameters describing the positions of the individual CCD chips with respect to the camera and the focal length are accessible for Principal Investigators in the ALOS Science Program. Using these metadata and an appropriate sensor model, direct geo-referencing is possible with an accuracy of about 50 m in object space (Weser et al., 2008).

Precise geo-referencing of high-resolution satellite images is essential to exploit the full geometric potential of the imagery for mapping and GIS applications. In our previous work (Weser et al., 2008) we have presented a generic pushbroom scanner model that is also suitable for ALOS PRISM data. In this model, the relative alignment of the CCD chips is described by six parameters per chip, namely the coefficients of two second-order polynomials. Using the metadata provided by JAXA and a small number of ground control points (GCPs), pixel-level results could thus be achieved for geo-referencing. The distribution of the resulting residuals in image space has suggested that the parameters describing the relative alignment of the CCD chips inside the cameras are not perfect and could be improved by on-the-job calibration. Such a calibration procedure has been described by Kocaman and Gruen (2007). Their sensor model also compensates for the displacement of the relative positions of the CCD chips by employing 6 additional parameters per image. Their results show that self-calibration improves the accuracy of geo-referencing to sub-pixel level. Tadono et al. (2007) present results of the self-calibration process at JAXA, correcting for the relative displacement of the CCD chips by using a linear regression model for each individual CCD chip. In JAXA (2006), the nominal lateral overlap of neighbouring CCD chips is given as 32 pixels, and no relative displacement in row direction is given. The results by Tadono et al. (2007) show that there are displacements of up to 2 pixels both in row and column direction compared to these nominal values.

This paper shows how the pushbroom sensor model described

* Corresponding author.

in Weser et al. (2008) has been expanded so that it can be used for on-the-job calibration of the relative alignment of the CCDs inside the cameras of ALOS PRISM. The initial values for these parameters are determined from information provided by JAXA in the form of camera coordinates of three points along each CCD chip. Two versions of these calibration data were received from JAXA: an early version in October 2006 and an updated version in July 2007. The results reported in Weser et al. (2008) were achieved using the older set of calibration data. In this paper we will compare the results achieved using both sets of calibration data. We will also present results of the on-the-job calibration of both data sets, and we will compare them to the original data. An evaluation of these results using check points will show the effectiveness of our own calibration procedure and also the effectiveness of the updated calibration carried out by JAXA.

2. THE PUSHBROOM SENSOR MODEL

At the Cooperative Research Centre for Spatial Information at the University of Melbourne (Australia) a generic pushbroom sensor model for high-resolution satellite imagery has been developed and integrated into the software system Barista (Barista, 2008). This sensor model will be described, with the focus being upon the requirements for precise georeferencing of ALOS PRISM imagery.

2.1 Transformation process

The physical model of the imaging process relates a point $\mathbf{P}_{ECS} = (X_{ECS},Y_{ECS},Z_{ECS})^T$ in an earth-centred object coordinate system to the position of its projection $\mathbf{p}_I = (x_I,y_I,0)^T$ in an image file coordinate *system*. A pushbroom scanner records each image row consecutively at time t while flying over the ground. The coordinate y_I of an observed image point therefore directly corresponds with the recording time t by $t = t_0 + \Delta t \cdot y_I$, where t_0 is the time of the first recorded image row and Δt the time interval for recording a single image row. The framelet coordinate system refers to an individual CCD array. In that coordinate system an image observation $\mathbf{p}_I$ can be expressed as $\mathbf{p}_F = (x_F,y_F,z_F)^T = (x_I,0,0)^T$. Each recorded image row is a central projection of the earth's surface recorded at time t that corresponds to y_I. The relation between an observed image point $\mathbf{p}_F$ in and the object point $\mathbf{P}_{ECS}$ is described by Equation 1:

$$\boldsymbol{p}_F = \boldsymbol{c}_F - \delta\boldsymbol{x} + \lambda \cdot \boldsymbol{R}_M^T \cdot \{\boldsymbol{R}_P^T(t) \cdot \boldsymbol{R}_O^T \cdot [\boldsymbol{P}_{ECS} - \boldsymbol{S}(t)] - \boldsymbol{C}_M\} \quad (1)$$

In Equation 1, $\mathbf{c}_F = (x_F^C,y_F^C,f)$ describes the position of the projection centre in the framelet coordinate system; its coordinates are usually referred to as the parameters of interior orientation: the principal point (x_F^C,y_F^C) and the focal length f. The vector $\delta\mathbf{x}$ formally describes corrections for systematic errors such as velocity aberration and atmospheric refraction. It can also be expanded to model camera distortion or other systematic effects. The shift $\mathbf{C}_M$ and the rotation matrix $\mathbf{R}_M$ describe a rigid motion of the camera with respect to the satellite. They are referred to as the *camera mounting* parameters. Since each image row is recorded consecutively while the satellite is moving, each image row also has its own exterior orientation corresponding to the acquisition time t. The satellite orbit path is modelled by time-dependant functions $\mathbf{S}(t) = [X(t), Y(t), Z(t)]^T$. The attitudes of the satellite orbit are described by a concatenation of a time-constant rotation matrix $\mathbf{R}_O$ and a matrix $\mathbf{R}_P(t)$ parameterised by time-dependant functions describing three rotation angles, *roll(t)*, *pitch(t)* and *yaw(t)*. The components of the orbit path and the time-dependant rotation angles are modelled by cubic spline functions. The rotation matrix $\mathbf{R}_O$ acts as an angular offset. It rotates from the earth-centred coordinate system to a system that is nearly parallel to the satellite orbit path and can be computed from the satellite position and velocity at the scene centre. Splitting the overall rotation into a time-constant and a time-dependant part prevents the parameterization of the time-dependant rotation matrix from becoming singular and leads to a more stable solution (Kim and Dowman, 2006).

A speciality of ALOS PRISM is that depending on the imaging mode four or six CCD chips are used to record a scene. This results in four or six sub-images that are delivered as separate image files for raw (level 1B1) data. These sub-images share their exterior orientation and camera mounting parameters and the focal length. However, each CCD chip has its own framelet coordinate system, and thus the coordinates of the principal point can be different for each of the sub-scenes. Figure 1 illustrates the configuration of four such CCD chips.

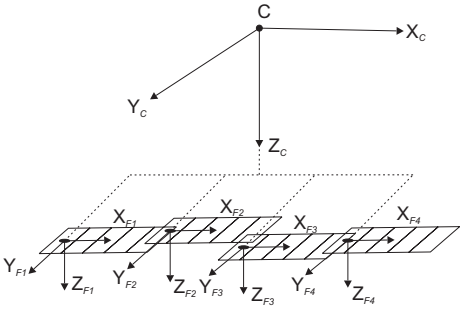

Figure 1.Configuration of four individual CCD chips of ALOS PRISM. (X_C, Y_C, Z_C): camera coordinate system.

In order to model this specific configuration, the bias correction vector $\delta\mathbf{x} = (\delta x, \delta y, 0)^T$ in Equation 1 is used. We still assume the coordinates of $\mathbf{c}_F = (x_F^C,y_F^C,f)$ to be identical for all sub-scenes. Then the corrections $(\delta x_i, \delta y_i)$ modelling the relative alignment of the CCD chips become:

$$\begin{aligned} \delta x_i &= \delta x_S + a_{0i} + a_{1i} \cdot x_{Fi} + a_{2i} \cdot x_{Fi}^2 \\ \delta y_i &= \delta y_S + b_{0i} + b_{1i} \cdot x_{Fi} + b_{2i} \cdot x_{Fi}^2 \end{aligned} \quad (2)$$

In Equation 2, i is the index of the CCD chip. The parameters δx_S and δy_S combine corrections for velocity aberration and atmospheric refraction. The constant coefficients a_{0i} and b_{0i} describe the relative shifts of the CCD chips. The coefficient a_{1i} is related to the pixel size, whereas b_{1i} models a shearing of the x_{Fi} axis. The second-order coefficient a_{2i} describes non-linear variations of the pixel size along the x_{Fi} axis, and b_{2i} models a deviation of the shape of the CCD chip from a straight line. Substituting Equation 2 into Equation 1 yields the modified version of the sensor model for ALOS PRISM.

2.2 Initialization of the sensor model parameters

There are two ways in which the parameters of the sensor model can be initialized. The minimum information required consists of the approximate focal length, the pixel size of the camera, the flying height of the satellite, and the two angles describing the viewing direction of the camera. This is sufficient to determine approximate values so that bundle block adjustment using a few GCPs will converge (Willneff et al.,

2008). However, many vendors of satellite imagery provide more precise information for initializing the model in metadata files. This is generally good enough for direct geo-referencing, within certain limits. As the definitions of the parameters describing the relationship between the object and the image coordinate systems vary between different vendors, so there is a requirement to map the vendor-specific definitions to those used in Equations 1 and 2. In Weser et al. (2008) we have described how this can be achieved for QuickBird, SPOT 5 and ALOS PRISM data.

In the case of ALOS PRISM, the camera mounting parameters and the orbit path and attitudes of the satellite are provided in the metadata files. The orbit path is represented by discrete points with a time stamp. The coefficients of the splines describing the components of $\mathbf{S}(t)$ and the time-constant rotation matrix $\mathbf{R}_O$ in Equation 1 can be determined from these points. The attitude information comes in the form of sets of quaternions describing an overall rotation matrix $\mathbf{R}_A(t)$ at discrete points in time. Each set of quaternions is used to determine a triplet of observed rotation angles using the identity $\mathbf{R}_A(t) = \mathbf{R}_O \cdot \mathbf{R}_P(t)$. These observations are used to determine the coefficients of the splines describing the rotational angles. The parameters of the interior orientation ($\mathbf{c}_F$ in Equation 1) and the information required to determine the coefficients a_{ji} and b_{ji} in Equation 2 are provided by JAXA. The CCD alignment is represented by coordinate tuples (X_C, Y_C) for three points of each CCD chip (leftmost, centre, and rightmost pixel) in the camera coordinate system (Weser et al., 2008).

2.3 Bundle adjustment with systematic error correction

The aim of bundle adjustment is to improve the parameters of the sensor model formulated in Equations 1 and 2 using the framelet coordinates of GCPs and tie points, the object coordinates of GCPs, and direct observations for the orbit path and attitudes derived from the metadata files. The camera mounting parameters ($\mathbf{C}_M$ and $\mathbf{R}_M$) and the parameters of the interior orientation ($\mathbf{c}_F$) cannot usually be determined given the small opening angles of the cameras and the small variations in height compared to the orbit height of the satellite. These parameters and the rotation matrix $\mathbf{R}_O$ are considered constant in adjustment. Assuming that no self-calibration is to be carried out, this leaves the coefficients of the spline functions modelling the time-dependant components of the orbit path $\mathbf{S}(t)$ and the time-dependant rotational angles parameterising $\mathbf{R}_P(t)$ to be determined in the adjustment. The adjustment model is expanded by parameters describing systematic errors in the direct observations for the orbit path and attitudes. For each orbit parameter p (the coordinate of an orbit point or a rotational angle), a time-constant unknown Δp is introduced. The observation p^{obs} recorded at time t^{obs} is related to the spline $S_p(t)$ describing the parameter p by:

$$S_p(t^{obs}) = p^{obs} + \Delta p \qquad (3)$$

This results in six parameters for systematic error correction per satellite orbit that have to be determined along with the spline parameters, namely three offsets $(\Delta X, \Delta Y, \Delta Z)^T$ for the orbit path points and three offsets $(\Delta roll, \Delta pitch, \Delta yaw)^T$ for the rotational angles. As there are substantial correlations between these correction parameters, which might lead to near-singular normal equation systems, it is advisable to add direct observations to the adjustment, observing each parameter to be 0 with a certain a priori standard deviation. In the case of ALOS PRISM, this a priori standard deviation is best selected to correspond to about 10 m in object space (Weser et al., 2008).

2.4 Self-calibration

In the case of bundle adjustment with self-calibration, the coefficients a_{ji} and b_{ji} in Equation 2 can be introduced as additional unknowns into the bundle adjustment. However, determining all these parameters for all CCD chips is equivalent to determining the interior orientation of the cameras. Thus, for each of the three cameras of PRISM, one CCD is selected as the master chip, whose alignment parameters are considered to be constant. The coefficients of all the other chips and, thus, their alignment relative to the master chip, are determined in adjustment. Systematic errors in the parameters of the master chip will be absorbed by the corrections to the exterior orientation parameters, just as are systematic errors in the camera mounting and interior orientation parameters. In our current implementation, the user is free to decide which of the coefficients in Equation 2 are to be treated as constant and which are to be determined in the adjustment. In addition, direct observations for the unknowns can be introduced in order to avoid singularities caused by parameters that cannot be determined from the observations.

3. EXPERIMENTS

3.1 The Melbourne test data set

For the experiments carried out for this study three ALOS PRISM scenes (forward, nadir, backward) covering Melbourne, Australia, have been used. Each scene consists of four separate image files and covers a total area of 40 x 49 km^2 with a ground resolution of 2.5 m. The in-track viewing angles of the scenes are 0º for nadir and ±23.8º for the forward and backward views. The images were recorded on 23 March 2007. The elevations in the test area range from sea level up to 200 m. Since the effective width of a PRISM scene is smaller than four times the size of a CCD chip, a large part of the outermost images does not actually contain data. This can lead to very narrow strips of real image data in the outermost image files, making it difficult to find features appropriate as GCPs or tie points (Figure 2).

In order to initialise the coefficients describing the relative alignment of the CCD chips, two sets of calibration data were made available by JAXA. The first set of calibration data was received in October 2006 and reflects a relatively early stage of calibration. An improved set of calibration data was received in July 2007. Both parameter sets are used in our experiments.

In the area covered by the three scenes, a test field consisting of 114 3D points was available. All points were surveyed by kinematic GPS with an accuracy of 20 cm in planimetry and 40 cm in height. In the inner city area as well as the surrounding suburbs the centres of road roundabouts were used. These are well defined in both object and image space. At the urban fringes road intersections had to be used for lack of other accessible features, which resulted in a somewhat poorer geometric definition of these points. The image coordinates of the centres of the roundabouts were determined from points measured around the perimeter using an ellipse fitting technique. The image coordinates were thus determined with a standard deviation of about 0.5 pixels.

3.2 Evaluation strategy

In order to carry out our tests, a set of 10 points of the Melbourne test field was selected to serve as GCPs for bundle adjustment. This number of GCPs has been shown to give pixel-level results for georeferencing without self-calibration (Weser et al., 2008). GCPs were chosen to be equally distributed over the scenes. The remaining 104 points were used as independent

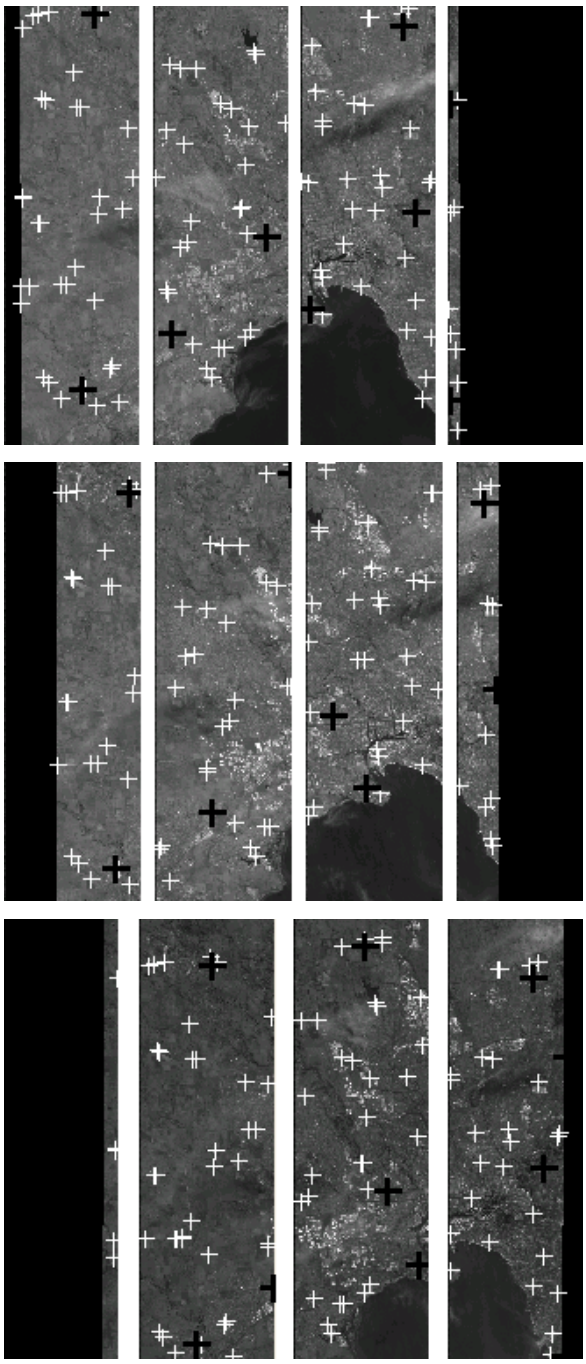

Figure 2.ALOS PRISM 1B1 images of Melbourne with four CCD chips. Black crosses: GCPs; white crosses: check points. Top is forward view, middle nadir view and bottom backward view.

checkpoints to assess and compare the accuracy achieved for georeferencing using different versions of bundle adjustment. In Figure 2, the GCPs are represented by black crosses, whereas the checkpoints are shown in white.

As mentioned earlier, some of the ALOS PRISM sub images contain only small stripes of data which also leads to a relatively small number of available check points. For the right most image file of the forward and nadir scene, eight check points could be employed whereas for the left most image file of the backward scene only six points were available. All other sub images are covered by 22 to 32 check points. In the adjustment, the check points were used as tie points, i.e. their object coordinates were determined. However, their GPS coordinates were not used as observations.

In the standard case of the adjustment, only the spline parameters modelling the exterior orientation, the bias correction parameters for the orbit path and attitude observations and the object coordinates of the check points and the GCPs are determined. For the self-calibration a second adjustment was carried out, determining, in addition to the unknowns in the standard case, the ALOS PRISM CCD chip alignment parameters. For the analysis in this work only the constant and linear coefficients (a_{0i}, b_{0i}, a_{1i} and b_{1i}) have been introduced as unknowns in the adjustment. Calibrating the quadratic coefficients would require a denser and better defined 3D point field in order to determine significant parameters. In all three scenes the second sub image was treated as the master CCD chip, whose alignment parameters remained constant. Therefore, for the self-calibration, 12 (four per sub image) additional CCD chip alignment parameters per scene were introduced. To avoid singularities in the adjustment direct observations with precision information for all 12 additional unknowns were introduced. The constant coefficients (a_{0i} and b_{0i}) were weighted according to a standard error of 1.5 pixels and the linear terms according to 300 ppm, an equivalent value considering the width of a single CCD chip. For a successful self-calibration it is important that a sufficient number of tie points is used.

For each set of CCD chip alignment parameters provided by JAXA first the standard adjustment is carried out followed by the self-calibration, which resulted in four different variants of adjustment. For the evaluation of the results in image space, the original check points were back projected into the images by using the adjusted projection parameters. The root mean square (RMS) error of coordinate differences was then computed by differencing the back projected check points and their image observations. In object space the RMS of object coordinate differences was computed by differencing the original check point coordinates with those determined during each adjustment. The differences in object space were computed in UTM coordinates. In addition to the RMS values, maximum residuals for both image and object space were determined.

3.3 Effects of self-calibration

The effectiveness of the self-calibration of the CCD chip alignment parameters is first analysed. For this purpose we are examining the changes in the calibrated CCD chip alignment parameters before and after self-calibration for both sets of parameters. For all three viewing directions similar changes can be observed, and thus the focus will be upon the representative nadir view direction. Figure 3 shows the arrangement of the CCD chips within the camera for both parameters sets. The continuous lines show the arrangement of original CCD chips whereas the dotted lines indicate the positions after the self-

calibration. When using the parameter set from October 2006, after self-calibration, changes between 0.1 and 0.8 pixels are observed for the along-track direction, whereas significant across-track changes of up to 2 pixels occur. Utilisation of the second set of parameters from July 2007 produces maximum changes of 0.5 pixels in-track and up to 2 pixels across-track, but in general changes are smaller than with the first set of parameters. In Figure 3 this can be seen especially for CCD chip 3 and for 4.

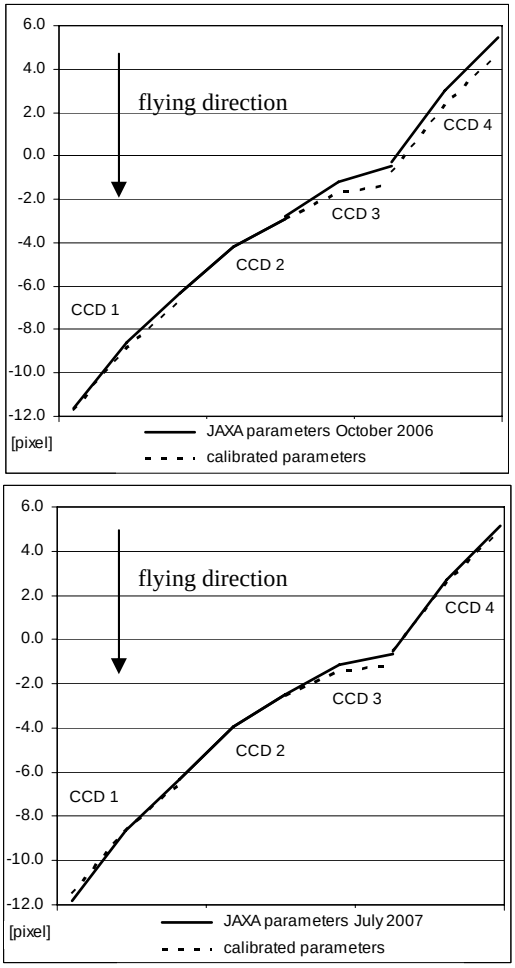

Figure 3.Arrangement of CCD chips within nadir camera. Continuous lines show original positions. Dotted lines show positions after self-calibration. Top: alignment parameters from October 2006; bottom: alignment parameters from July 2007.

The effect of the self-calibration shall now also be analysed by comparing the RMS values as well as the maximum residual, computed for each sub image and for all four adjustments summarized in Tables 1 to 3. When using the CCD chip alignment data set from 2006, a similar pattern can be observed when no self-calibration is applied for all three cameras. For each camera the RMS values of the inner sub images are between 0.3 and 0.8 pixels whereas for the outer sub images RMS values between 0.6 and 1.6 have been computed, suggesting a systematic misalignment of these CCD chips. When applying the self-calibration a significant improvement can be observed for most of the CCD chips, especially for the outer sub images. Only sub image '2' of the backward camera shows an increased RMS value. In this sub images no GCP could be measured due to the lack of features. Therefore it only takes part in the calibration process via the tie points. The maximum residuals are between 0.6 and 2.4 pixels with and without self-calibration. When self-calibration is carried out a slight decrease in the outer sub images can be observed. It is noteworthy that most of the outliners occur at road intersections and therefore reflect the poor definition of these points.

Utilizing the second set of parameters decreases the already mentioned pattern drastically but it can still be observed. The RMS values of the inner sub images are now between 0.4 and 0.7 pixels and for the outer images between 0.6 and 0.9 pixels. With the exception of sub image '2' of the backward camera an improvement can be observed when self-calibration is applied, showing RMS values between 0.3 and 0.9 pixels and a more consistent distribution over all sub images.

parameters		Oct 2006		July 2007	
calibration		no	yes	no	yes
CCD id		RMS/R_{max}	RMS/R_{max}	RMS/R_{max}	RMS/R_{max}
2	x	0.96 / 1.74	0.63 / 1.98	0.86 / 1.61	0.64 / 2.08
	y	0.84 / 2.15	0.66 / 1.88	0.79 / 2.01	0.67 / 1.99
3	x	0.38 / 1.00	0.37 / 1.07	0.40 / 0.81	0.34 / 0.97
	y	0.50 / 1.02	0.49 / 1.01	0.53 / 1.00	0.49 / 1.00
4	x	0.52 / 1.28	0.47 / 1.17	0.52 / 1.12	0.49 / 1.19
	y	0.67 / 1.34	0.66 / 1.32	0.67 / 1.40	0.66 / 1.28
5	x	1.00 / 1.74	0.82 / 1.88	0.90 / 1.75	0.81 / 1.91
	y	0.80 / 1.08	0.31 / 0.48	0.70 / 1.00	0.32 / 0.47

Table 1. Results of forward scene for all four adjustments. RMS values and maximum residuals are shown in pixels.

parameters		Oct 2006		July 2007	
calibration		no	yes	no	yes
CCD id		RMS/R_{max}	RMS/R_{max}	RMS/R_{max}	RMS/R_{max}
1	x	0.95 / 2.18	0.57 / 1.09	0.84 / 1.92	0.58 / 1.17
	y	0.86 / 2.16	0.82 / 2.34	0.85 / 2.36	0.82 / 2.37
2	x	0.70 / 1.27	0.50 / 0.86	0.46 / 0.88	0.46 / 0.86
	y	0.30 / 0.72	0.32 / 0.60	0.32 / 0.74	0.35 / 0.82
3	x	0.74 / 1.77	0.64 / 1.96	0.66 / 2.17	0.63 / 2.01
	y	0.51 / 1.44	0.40 / 1.10	0.43 / 1.32	0.40 / 1.07
4	x	1.60 / 2.27	0.47 / 0.87	0.79 / 1.32	0.45 / 0.78
	y	0.94 / 2.10	0.86 / 1.82	0.89 / 1.82	0.87 / 1.83

Table 2. Results of nadir scene for all four adjustments. RMS values and maximum residuals are shown in pixels.

parameters		Oct 2006		July 2007	
calibration		no	yes	no	yes
CCD id		RMS/R_{max}	RMS/R_{max}	RMS/R_{max}	RMS/R_{max}
2	x	1.06 / 1.55	1.16 / 1.96	0.99 / 1.28	1.21 / 2.05
	y	0.90 / 1.53	0.90 / 1.72	0.91 / 1.64	0.93 / 1.82
3	x	0.85 / 1.83	0.52 / 1.29	0.63 / 1.62	0.53 / 1.38
	y	0.72 / 2.33	0.64 / 2.11	0.71 / 2.24	0.61 / 2.02
4	x	0.50 / 1.20	0.52 / 1.19	0.47 / 1.12	0.49 / 1.12
	y	0.45 / 1.28	0.44 / 1.11	0.46 / 1.41	0.47 / 1.06
5	x	0.66 / 2.42	0.62 / 2.34	0.65 / 2.46	0.63 / 2.39
	y	0.61 / 1.73	0.56 / 1.51	0.71 / 1.99	0.58 / 1.54

Table 3. Results of backward scene for all four adjustments. RMS values and maximum residuals are shown in pixels.

A comparison between both original parameter sets from JAXA shows an improvement in the RMS values over all sub images and for all viewing directions and therefore shows that the recalibration carried out by JAXA has been successful. The results for both data sets are almost identical when our self-calibration is applied.

3.4 Assessment of the geo-referencing accuracy

The RMS values in 3D, along with the maximum residuals, for both sets of parameters with and without self-calibration, are listed in Table 4. For the early set of CCD alignment parameters, RMS values below 2.0 m in planimetry and up to 2.3 m in height are obtained when no calibration is applied. The determination of additional parameter has yielded significant improvements. RMS values are now below 1.5 m in planimetry and 1.7 m in height, an improvement of about 33 % in both components. When utilizing the second set of parameters the RMS values in planimetry are below 1.6 m and 2.1 m in height without self-calibration. With self-calibration we observe again an improvement, however it is less significant. The RMS is now 1.5 m and below in planimetry and 1.7 m in height. As in 2D, points with the largest residuals are mainly those at road intersections.

Comparing the results between the two sets of parameters shows a clear improvement in planimetry and height when utilizing the alignment data from 2007. The RMS discrepancy drops from 2.0 m to below 1.6 m in planimetry and from 2.3m to 2.1 m in height, an improvement of 25 % and 9 %, respectively. Again, this shows that the recalibration carried out by JAXA has been successful. The determination of additional parameters yields almost identical results for both cases and the RMS values in planimetry and height are significantly smaller than without self-calibration.

parameter set	calibration	planimetry		height
		X [m]	Y [m]	Z [m]
		RMS / R_{max}	RMS / R_{max}	RMS / R_{max}
Oct 2006	no	1.98 / 5.24	1.44 / 4.51	2.29 / 7.24
Oct 2006	yes	1.47 / 5.60	1.30 / 5.22	1.68 / 5.59
July 2007	no	1.58 / 5.20	1.37 / 4.82	2.10 / 5.00
July 2007	yes	1.47 / 5.87	1.31 / 5.29	1.71 / 5.92

Table 4. Results of geo-referencing in 3D. RMS and maximum residuals are shown in UTM.

3.5 Discussion

Sub-pixel 3D georeferencing accuracy has been achieved for both sets of parameters, regardless of whether calibration is applied or not. It has been shown that utilisation of the second set of parameters yields a significant accuracy improvement in planimetry and height and thus shows that the new calibration carried out by JAXA has been successful. Determination of the proposed additional parameters further improves the results in both cases, which illustrates that additional calibration is possible and necessary in order to achieve the full geopositioning potential of ALOS PRISM imagery. Especially in image space, a clear enhancement for the outer sub images can be observed. The systematically higher RMS values for all outer sub images were reduced when using the second set of parameters, and sub-pixel accuracy was achieved for all images. The proposed self-calibration can further improve the attainable accuracy. Only sub image '2' of the backward camera shows increased RMS values, which can be explained by a lack of GCP information. Overall, the proposed self-calibration leads to almost identical results for both sets of JAXA parameters, which shows that a stable, equally accurate solution can be arrived at from both sets of JAXA calibration parameters.

4. CONCLUSION

In this paper we have presented the successful self-calibration of ALOS PRISM imagery with our generic pushbroom sensor model by using additional parameters. With the improved pushbroom sensor model, sub-pixel georeferencing accuracy for the 2.5 m imagery been achieved. We can also confirm that the newer of the two sets of CCD chip alignment parameters provided by JAXA provides a considerable accuracy improvement over the original set from October, 2006. However, our results also demonstrate that a further refinement of calibration parameters can still lead to improved georeferencing results. Further research is required to ascertain whether the additional parameters determined in the reported self-calibration can be used to improve the georeferencing in other scenes.

ACKNOWLEDGEMENTS

The authors would like to express their thanks to JAXA for providing the information required to instantiate the parameters describing the relative alignment of the CCD chips.

REFERENCES

Barista, 2008. Barista product information webpage, *http://www.baristasoftware.com.au* (Accessed: 21. April 2008).

Jaxa, 2006. ALOS Product Format Description. *http://stage.tksc.jaxa.jp/eorcalos/PRISM_L1_J_ENa.zip* (Accessed: 7. April 2007)

Kim, T., Dowman, I., 2006. Comparison of two physical sensor models for satellite images: Position-Rotation model and Orbit-Attitude model. *Photogrammetric Record*, 21(114): 110-123.

Kocaman, S. and Grün, A., 2007. Rigorous sensor modelling of ALOS/PRISM imagery. *Proceedings of the 8th Conference on Optical 3D Measurement Techniques*, Zurich, Switzerland, 204-212.

Tadono, T., Shimada, M., Iwata, T., Takaku, J., 2007. Accuracy assessment of geolocation determination for PRISM and AVNIR-2 onboard ALOS. *Proceedings of the 8th Conference on Optical 3D Measurement Techniques*, Zurich, Switzerland, 214-222.

Weser, T., Rottensteiner, F., Willneff, J., Poon, J., Fraser, C., 2008. Development and testing of a generic sensor model for high-resolution satellite imagery. *Photogrammetric Record* (in press).

Willneff, J., Weser, T., Rottensteiner, F., Fraser, C., 2008. Precise georeferencing of Cartosat imagery via different orientation models. Accepted for oral presentation at the ISPRS Congress in Beijing, *Intern. Arch. of Photogrammetry, Remote Sensing & Spatial Information Sciences*, SS 11 (Cartosat-SAP).